ISSN: 1410-8917
Jurnal Kimia Sains & Aplikasi
e-ISSN: 2597-9914

Jurnal Kimia Sains dan Aplikasi 26 (8) (2023): 300-309

Jurnal Kimia Sains dan Aplikasi
Journal of Scientific and Applied Chemistry

Journal homepage: http://ejournal.undip.ac.id/index.php/ksa

Combined Classical and Flooding Molecular Dynamics Simulations of The Mip-Rapamycin and FKBP12-Rapamycin Complexes

Elisabeth Catherina Widjajakusuma [1,*], Monica Frederica [1], Kornelius Kaweono [1]

[1] Faculty of Pharmacy, Widya Mandala Catholic University, Surabaya, East Java, Indonesia

* Corresponding author: ecwidj@ukwms.ac.id

https://doi.org/10.14710/jksa.26.8.300-309

Article Info

Article history:

Received: 06th June 2023
Revised: 04th November 2023
Accepted: 09th November 2023
Online: 15th November 2023

Keywords:
macrophage infectivity potentiator; *Legionella pneumophila*; FKBP12, conformational flooding; dihedral angle principal component analysis

Abstract

Macrophage infectivity potentiator (Mip) protein, an essential virulence factor encoded by pathogenic bacteria such as *Legionella pneumophila*, arises as an interesting new therapeutic target for novel antimicrobials. However, Mip- ligands also interact with FKBP12 protein, a human FKBP exhibiting immunosuppressive effects. Therefore, these ligands are unsuitable antibiotics. Understanding the dynamics and conformations of proteins in the binding pocket is important to predict binding properties and to design new binders for different FKBPs. We performed the 40 ns combined classical and flooding molecular dynamics simulations using additional flooding potential for Mip-rapamycin and FKBP12-rapamycin complexes. Both complexes have different flexibilities and dihedral angle principal component analysis calculated from MD trajectories. As a result, the Mip-rapamycin complex had more conformations than the FKBP12-rapamycin complex. These different features of both complexes at the binding pocket will provide new dues for the design of selective inhibitors of Mip proteins.

1. Introduction

Legionella pneumophila is the most common species, a gram-negative intracellular facultative pathogen that causes 90% of the cases of legionellosis [1]. This virus causes severe multisystem disease, consolidating pneumonia, and extrapulmonary infections, such as endocarditis or wound infections [2, 3]. Symptoms of Legionnaires' disease include fever, malaise, myalgia, fever, chills, headache, and nonproductive cough [3, 4]. Freshwater biofilms support the proliferation of *L pneumophila* that replicate inside free-living amoebae. The transmission of the disease occurs when persons come into contact with artificial water systems that *L pneumophila* colonizes. Bacteria present in shower heads, hot-water faucets, and air-conditioning units facilitate the entry of bacteria into the human lungs [5, 6]. The macrophage infectivity potentiator (Mip) protein of *L. pneumophila* is associated with the major virulence factor and classified within the enzyme family of FK506-binding proteins (FKBP), which exhibits peptidyl-prolyl-*cis/trans* isomerase (PPIase) activity. The PPIase domain of the Mip protein of *L. pneumophila* is structurally highly similar to human FKBP12; both proteins interact with rapamycin [7, 8].

FKBP12, a 12 kDa protein, was the first one described in 1989 as the most abundant and the smallest member of the FKBP family [9, 10, 11]. Rapamycin binds noncovalently to FKBP12, and subsequently, the rapamycin-FKBP12 complex targets the mammalian target of rapamycin (mTOR) [12, 13, 14, 15]. Therefore, the inhibition of FKBP12 alone does not contribute to their immunosuppressive activity; instead, the immunosuppression is facilitated by FKBP12 by inhibiting mTOR [15]. Due to its immunosuppressive effect, rapamycin is clearly counterproductive for the treatment of Legionnaire's disease. These data prompt the development of Mip inhibitors that do not interfere with immune responses [16].

Molecular dynamic (MD) simulations have been applied widely and successfully to numerous drug discovery processes [17, 18, 19, 20]. A combination of NMR relaxation analysis and molecular dynamics trajectories of the homodimeric Mip protein provides insight into the local dynamics and residual coupling between domain motions [7]. Changes in protein

conformational dynamics of the FKBP12-FK506 complex were also shown by a combined NMR-MD approach [21]. Moreover, MD simulations of a binding intermediate state between the protein FKBP12 and a high-affinity ligand allow a rational explanation for the diversity of the core and non-core structures found in various high-affinity ligands of FKBP12 [22].

MD simulations of both complexes were performed in this study to investigate dynamic interactions between residues of the proteins (Mip of *L. pneumophila* and FKBP12) and atoms of rapamycin. However, the timescale to study and predict conformational motions or structural transitions in macromolecular systems (especially in proteins) on a microsecond time scale is far beyond what classical MD can address [23]. To overcome this problem, this study used principal component analysis coupled with conformational flooding. The basic principle in conformational flooding is to destabilize a local minimum structure by adding a flooding potential that stimulates the simulated system to explore new regions of phase space in a short simulation time [24, 25, 26].

2. Experimental

2.1. The Simulation Systems

The initial conformations of the complexes were taken from 2VCD [7] and 1FKB [8]. Ligands were parameterized with the general AMBER force field (GAFF), and the charges were derived using the AM1-BBC method implemented in the Antechamber program [27] of the AMBER18 [28]. GROMACS topologies and coordinates were generated from the AMBER18 ones using acpype [27, 29, 30]. The simulations were performed in GROMACS version 2018.2 [31, 32, 33, 34, 35, 36, 37, 38] using the Amber99SB force field [39]. The Mip-rapamycin and FKBP12-rapamycin complexes were then neutralized using 4 Cl^- and 1 Cl^- counterions and solvated with 8486 and 6430 explicit TIP3P waters [40], respectively, in a decahedron box that extended 10 Å beyond any complex atom.

The velocity Verlet algorithm with a 2 fs timestep was used to integrate the equations of motion. Periodic boundary conditions were applied. The particle-mesh Ewald method [41] for Ewald sums in large systems with a 12 Å direct space cutoff distance was employed for the long-range electrostatic interactions. The temperature of the system was kept at 300 K using the V-rescale method [42], and the pressure was kept at 1 bar using the Parrinello-Rahman method [43]. The length of the bonds involving hydrogen atoms was constrained using LINCS [34].

2.2. Molecular Dynamics Simulations

The molecular dynamics (MD) simulation process consisted of six steps: minimization, equilibration using the canonical NVT (constant number of particles, volume, temperature) ensemble, then the NPT (constant number of particles, pressure, and temperature) ensemble, production dynamics using isothermal isobaric (NPT) ensemble, production dynamics with conformational flooding, and finally production dynamics without conformational flooding. First, the system was minimized for 50,000 steps of steepest descent minimization. Second, the systems were equilibrated using the NVT ensemble for 50,000 steps (100 ps) and then the NPT ensemble for an additional 50,000 steps (100 ps). Production dynamics were then performed using the isobaric-isothermal NPT (constant number of particles, pressure, and temperature) ensemble using a 2 fs time step, and coordinates were saved every pico second for analysis during 10 ns. The SHAKE algorithm was used to constrain the motion of hydrogen-containing bonds [44, 45].

Long-range electrostatic interactions were calculated using the particle mesh Ewald (PME) method [46]. As protein dynamics are influenced by their energy surface, introducing potential energy can accelerate these processes. The flooding potentials were used to gain insight into the dynamics of the complex [24, 25, 47, 48]. In this study, adaptive flooding with a target destabilization-free energy ΔF_0 = 150 kJ/mol, the initial flooding strength $E_{fl}^{(0)}$ = 0, and a time constant τ = 0.1 ps was employed on the complexes. A 10 ns trajectory of the system was used for the principal component analysis (PCA).

The flooding potential was built on combinations of these PCA eigenmodes. The destabilizing forces were applied to all atoms. Subsequently, a flooding simulation was conducted for 10 ns. Finally, an additional molecular dynamics (MD) simulation without the flooding potential was performed for 20 ns. The results of the simulations were analyzed by dihedral angle principal component analysis (dPCA) to reduce the dimensionality of MD data [49, 50]. The dPCA uses the sine/cosine-transformed φ and ψ dihedral angles of the peptide backbone to separate the internal and overall dynamics of the conformations.

3. Results and Discussion

3.1. Overall Dynamics Behavior

The conformational change and the conservation of the protein structure were monitored by the time evolution of all atoms and the backbone atoms' root-mean-square deviation (RMSD) relative to their initial energy-minimized structure and by the calculation of the root-mean-square fluctuation (RMSF) through the 40-ns simulations of both complexes (Figure 1). The flooding simulations were performed between 10–20 ns for both simulations. RMSD and RMSF of the structures are the most common mobility measures. Elevated RMSD and RMSF values indicate greater mobility, while lower values suggest reduced mobility.

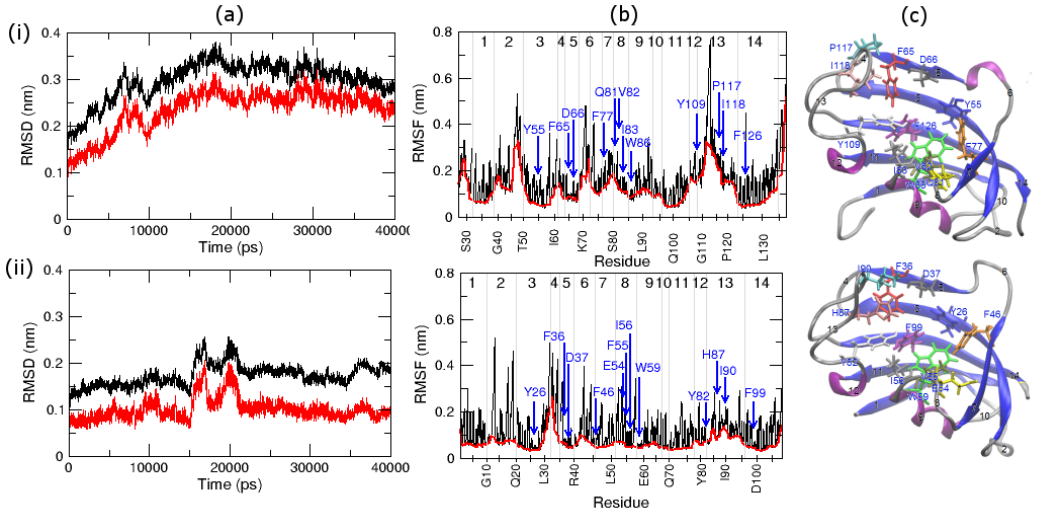

Figure 1. Structural analysis of the Mip (i) and FKBP12 (ii) proteins. (a) Root-mean-square deviation (RMSD) of all atoms (black lines) and backbone atoms (red lines) with respect to their initial energy minimized structure as a function of time. (b) RMSFs of all atoms (black lines) and backbone atoms of individual residues (red lines) during 40-ns MD simulations. The locations of the protein secondary structural elements are numbered according to the protein structure on the right side, and the locations of the residues in the binding pocket are marked in the figure. (c) The initial structure of the proteins. Coils, sheets, and helices are represented in gray, blue, and purple, respectively. The residues in the active site are depicted in colored sticks

Root-mean-square deviation (RMSD) is a parameter that indicates how much a structure differs from its reference structure. Therefore, it is considered an important indicator for evaluating the stability of a protein in terms of structural conformation. RMSD was calculated for all atoms and backbone atoms of both proteins to provide an overall measure of the departure of the structures from the initial coordinates. Despite the global structural similarities and their shared capability to bind rapamycin within a similar binding site, Figure 1(a) clearly illustrates differences in the mobility of the two proteins. Mip protein showed a higher value of 3.8 Å around 18 ns, followed by a gradual convergence to the range of 2.8 to 3 Å as the simulation progresses (Figure 1 (i-a)). Conversely, RMSD fluctuations reaching 2.5 Å were observed at 15–22 ns for FKBP12. However, most of the time, the RMSD values of FKBP12 remained in the range of 1.5 to 2 Å over the 40 ns simulation (Figure 1 (ii-a)). The difference in RMSD values between Mip and FKBP12 proteins suggests that Mip has more flexible domains than FKBP12, which was corroborated by the RMSF analysis.

The local and diagnostic dynamics of each residue were assessed based on the root mean square fluctuations (RMSF) of all atoms for both proteins. The RMSFs in Figure 1(b) show that the main conformational stability differences between both proteins were associated with the regions 2, 4, 6, 7-8, and 13 around rapamycin. The secondary structures of the proteins shown in Figure 1(c) are numbered sequentially from the N-terminus to the C- terminus. Residues 1 to 26 of the Mip protein are omitted, with residues occupying corresponding positions in the hydrophobic cavity of both proteins depicted in the same colors. The RMSF comparison between Mip and FKBP12 indicates a substantial disparity in the conformational stability of the two proteins. An examination of the structural flexibility of both proteins reveals that Mip had a higher average value of RMSF (1.7 Å) compared to FKBP12 (1.2 Å).

Previous studies showed a minor structural rearrangement upon binding rapamycin with Mip in regions 7-8 and 13, which was less marked in FKBP12 [7, 8]. Furthermore, the relative higher fluctuations of FKBP12 in the region and 6 were confirmed by B-factor analysis [51]. In region 13, three residues—namely, Y109, P117, and I118 for the Mip protein, and Y82, H87, and I90 for FKBP12—are involved in the binding interaction. The high fluctuation of Mip might explain a lower binding affinity between the protein and rapamycin.

3.2. Effect of Conformational Flooding

Dihedral angle principal component analysis (dPCA) was conducted to remove rotations and translations of the MD simulations. Additionally, it was used to analyze and visualize the MD trajectories in conformational space (Figure 2). All the structures obtained from the MD simulations were projected onto the first two principal components (PC1 and PC2). As represented in Figure 2, most conformations form clusters representing a collection of similar conformations. PC1 went from negative to positive values in both simulations, as shown in Figure 2(a).

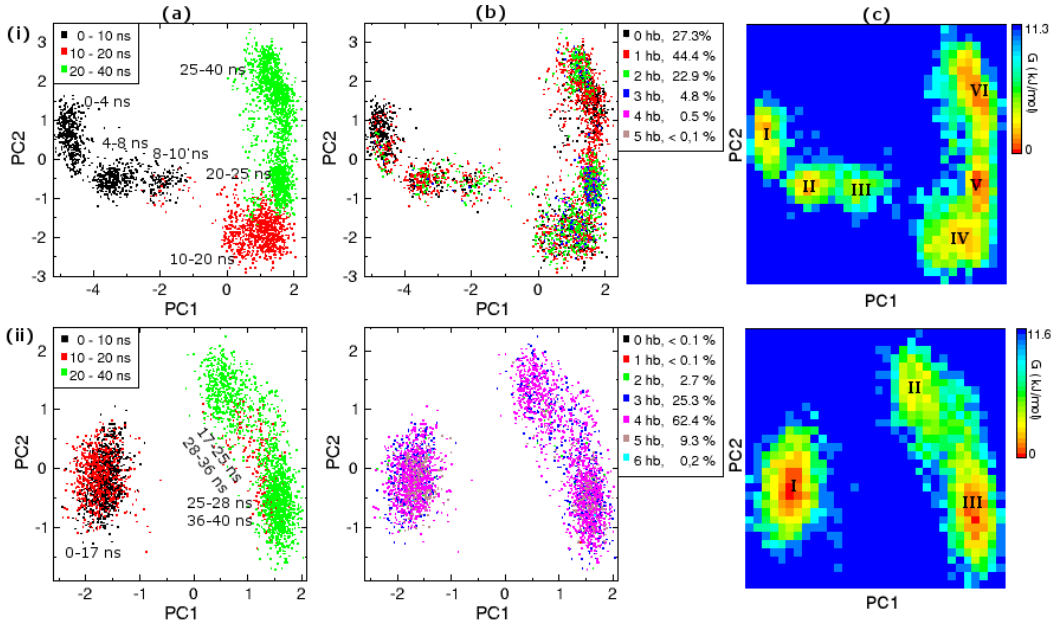

Figure 2. Dihedral angle principal component analysis of Mip (i) and FKBP (ii) proteins along the first two principal eigenvectors. (a) The colors, as given in the legend, correspond to time evolution before (black), during (red), and after (green) flooding simulations. The estimation of the simulation time of each cluster was indicated. A period of time spent moving between two clusters was written diagonally. (b) The colors and occupancies in the legends indicate the number of hydrogen bonds. (c) Two-dimensional representation of the free energy landscape G (in kJ/mol). Their basins are roughly estimated and indicated by capital Roman numerals

However, the 2D projection in phase space of the Mip shows a gradual migration of the points (Figure 2(i-a)), indicating that the conformational flooding caused the protein to undergo more flexible motions than FKBP12 (Figure 2(ii-a)). It can be seen that the conformational flooding caused a larger fluctuation in Mip between 10 and 20 ns compared to FKBP12. There were three clusters before flooding (black points), one during flooding (red), and two after flooding (green) for Mip, while FKPB had only one cluster before flooding and two clusters after flooding with no special cluster during flooding. This indicates that Mip had more local minimums with lower energy barriers than FKBP12.

The number of hydrogen bonds between the proteins and rapamycin was also projected onto the two-dimensional subspace in Figure 2(b), demonstrating a non-homogeneous distribution for Mip and a homogeneous one for FKBP12. This suggests that the relative stability of the clusters was different for Mip, whereas FKBP12 had clusters with similar stability. The Mip-rapamycin also revealed that before the flooding simulation, the complex experienced fewer hydrogen bonding interactions represented by black and red colors, during the flooding green and blue, and after flooding red and green. On the contrary, the number of hydrogen bonds between FKBP12 and rapamycin was observed to be fairly constant, as shown by the magenta color representing four hydrogen bonds.

The free energy landscapes for PC1 and PC2 were also calculated and are shown in Figure 2(c). It can be observed that the Mip-rapamycin complex had a lower energy value ranging from 0 to 11.3 kJ mol^{-1} (Figure 2(i-c)) compared to the energy value of FKBP-rapamycin ranging from 0 to 11.6 kJ mol^{-1} (Figure 2(ii-c)) which suggests that conformational changes of Mip-rapamycin were energetically more favorable. Six and three local minima were identified for Mip-rapamycin and FKBP12-rapamycin, respectively, and marked by capital Roman numerals. Two metastable states (III and IV) during the conformational transitions of Mip-rapamycin were shown along the transition pathways caused by conformational flooding before reaching thermodynamically more favorable states (V and VI). In contrast, only one metastable state II was found during conformational changes of the FKBP12-rapamycin complex. The energy barrier between states II and III was not high enough, so the simulation moved between the two states in certain periods.

The global minimum states were reached after flooding or in around 24 ns (state V) and 34 ns (state VI) for Mip, but before flooding in around 3 ns (state I) and during flooding in around 17 ns (state II and III) for FKBP12. In summary, the flooding simulation facilitated conformational changes in the complexes, resulting in new and stable protein structures, as there was no regression towards the original structure after flooding.

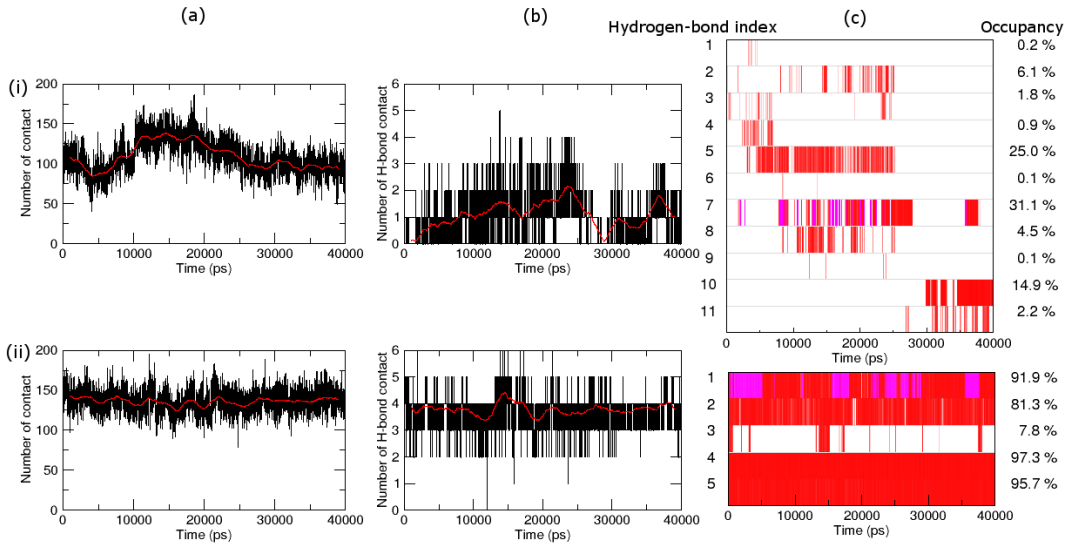

Figure 3. Intermolecular interactions between rapamycin and Mip (i) and FKBP12 (ii) proteins during MD simulations. (a) Number of van der Waals contact within the cutoff distance of 3.5 Å, and (b) number of hydrogen bonds as a function of time. The red lines show a 2000-ps running average. (c) Hydrogen-bond existence map for specific contacts of rapamycin with the residues in the binding pocket along MD simulations. Red lines indicate the presence of hydrogen bonds for particular interactions labeled by the same index in Figure 4 and their occupancies, and white breaks imply the absence of that hydrogen bond. Magenta lines refer to a hydrogen bond with the other oxygen atom from a carboxyl group of an aspartate side chain

3.3. Protein-Rapamycin Interactions at the Binding Pocket

The crucial interactions for ligand binding include intermolecular hydrogen bonding with the target protein and van der Waals interactions. Although van der Waals interactions are individually weak, the combined effect of multiple van der Waals interactions often contributes to the formation of highly stable and specific associations between the protein and ligand [52]. To verify intermolecular interactions between the proteins and rapamycin, the total number of hydrogen-bond and van der Waals (cutoff of 3.8 Å) contacts were calculated, and the results are shown in Figures 3(a) and (b), respectively. It can be seen that either the hydrogen-bond or van der Waals interactions existed more in FKBP12-rapamycin, observed with average numbers of 3.79 and 136, respectively, than in Mip-rapamycin with average numbers of 1.07 and 109. This implies that FKBP12-rapamycin has a higher binding affinity than Mip-rapamycin, explaining why rapamycin is unsuitable for *L. pneumophila* [16, 53].

The snapshots (Figure 4) of the complexes extracted from the basin of local minima in Figure 2(c) give a visual impression of the protein-rapamycin interactions and the dynamics of the process. The residues in the binding site were identified using Discovery Studio Visualiser [54], and the VMD program [55] was used for visualization. According to the hydrogen bond interaction of the snapshots (Figure 4), the hydrogen bond contacts were selected, labeled with numbers, and shown in Figure 3(c) with their occupancy. In the NMR structure of Mip-rapamycin, only one hydrogen-bond contact is detected (hydrogen-bond index 1 in Figure 3(i-c) and Figure 4(i: state I)). In comparison, in the first basin of cluster I, only one hydrogen-bond contact (hydrogen-bond index 2 in Figure 3(i-c) and Figure 4 (i: state II)) was also detected, albeit different from the previous one. These results confirm the dPCA analysis, where the conformation with no hydrogen bond contact and one hydrogen-bond contact were dominant in the first cluster (Figure 2(i-b)). Both hydrogen-bond contacts were not found in the following basins, indicating a different conformation.

In the next basin of state II, the snapshot showed more hydrogen-bond contacts and one of them belonged to the most occupied hydrogen-bond contacts between oxygen atom in the peptide bond of residue S113 and atom hydrogen of the hydroxyl group at the cyclohexyl ring (index 5 with 25% occupancy) that existed in the basins of state II to state V. The third snapshot was extracted from the basin of metastable state III, where the two most highly occupied hydrogen-bond (index 5 and 7 with 31.1% occupancy) contacts existed to stabilize the structure. The hydrogen-bond index 7 was formed by atom oxygen from the side chain of residue D66 and atom hydrogen from the hydroxyl group of the pyranosyl ring.

Figure 4. Snapshot for each basin in Figure 2(c) of Mip-rapamycin (A) and of FKBP12-rapamycin (B) complexes. The residues involved in the interaction are green for classical and light green for non-classical hydrogen bonding. The hydrophobic-bonding interactions are shown as purple for pi-sigma and pink for alkyl

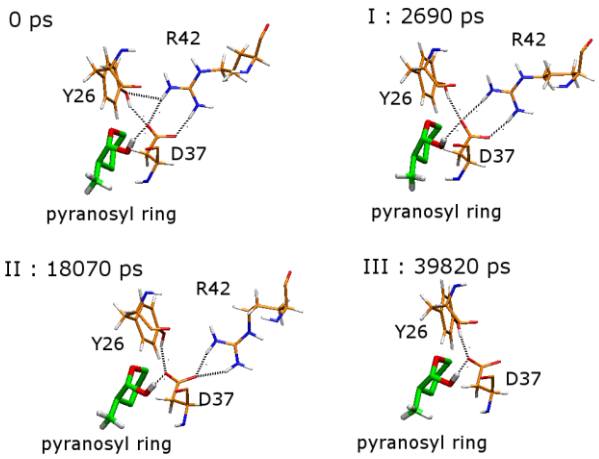

Figure 5. Intramolecular interaction at the binding pocket of FKBP12-rapamycin complex

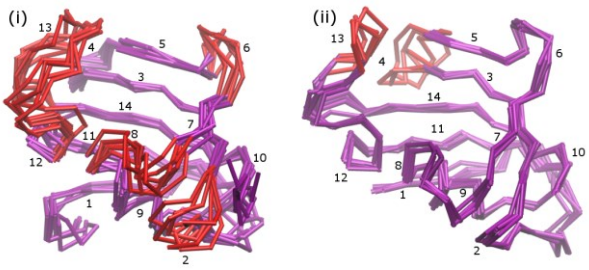

Figure 6. The superpositions of the backbones of Mip (i) and FKBP12 (ii) proteins. Purple and red colors show the slightly and highly mobile parts of the backbones, respectively. Each part of the proteins is numbered 1 to 14 with the same position shown in Figure 1

The fourth snapshot obtained during flooding showed more hydrogen-bond contacts with a new hydrogen bond (index 8 with 4.5%) between the hydrogen atom of the Q81 side chain and the oxygen atom of the hydroxyl group at C28. This contact existed during 10- 25 ns simulation time (Figure 3(i-c)), showing its presence in clusters 4 and 5 (Figure 2(i-b)) as well, indicating its crucial role in stabilizing rapamycin in the binding pocket. The sixth snapshot was quite different from the others, where a new and strong hydrogen-bond contact (index 10 with 14.9% occupancy) was involved between the hydrogen atom of the peptide bond of Q78 and the oxygen atom of the hydroxyl group at the cyclohexyl ring. The other weaker hydrogen bond contact (index 11 with 2.2% occupancy) was formed between the oxygen atom of the Q81 side chain and the hydrogen atom of the hydroxyl group at the cyclohexyl ring. Clusters 5 and 6 had the lowest energy conformers among the six local minima.

On the other side, the snapshots of FKBP12-rapamycin at the binding pocket show different hydrogen-bond contact features in Figures 3 and 4 from those of Mip-rapamycin. At the beginning of the simulation, before the flooding, FKBP12-rapamycin reached equilibrium with the lowest energy conformer (state I in Figure 2(ii-c)). The starting structure and first snapshot extracted from cluster I had only one insignificant difference in hydrogen-bond contact, which was the contact with 7.8% occupancy between the hydrogen atom of the hydroxyl group at C28 and oxygen atom in the peptide bond of E54 (hydrogen-bond index 3 in Figure 3(ii-c)). Four of five hydrogen-bond contacts existed in all states with occupancy of more than 80%

(Figure 3(ii-c)). The intramolecular hydrogen-bond interactions formed by residue Y26, D37, and R42 are shown in Figure 5. These interactions involving a water molecule trapped in the binding pocket, forming a hydrogen bond with the hydrogen atom of the peptide of residue E54, are responsible for the rigidity of the binding pocket. Notably, no significant changes were observed among the conformers of the three states.

In Figure 6, the superposition of the backbone of the conformers of all states obtained from dihedral angle principal component analysis revealed the flexible regions of the protein and agreed with RMSF calculations in Figures 1(b) and (c). In the case of Mip-rapamycin, regions 8 and 13 encompassed flexible residues engaged in interactions with rapamycin (Table S.1 in Supplementary Material for a summary of interactions within the binding pocket for both complexes). On the contrary, the three conformers of FKBP12-rapamycin demonstrated a similar pattern in the binding pocket. The main difference between the conformers was caused by the flexibility of region 4, which did not contain any residue involved in the hydrogen-bond interactions at the binding pocket, and region 13, which contained Y82, H87, I90, and I91 with the same interaction with rapamycin during the simulations (Table S.1 in Supplementary Material).

In general, the binding domain of rapamycin consists of the ester linkage, the pipecolyl ring, the dicarbonyl group, and the pyranosyl ring. This is consistent with the previous study of Ceymann *et al.* [7], where the pipecolyl ring invaded the hydrophobic cavity and was surrounded mainly by aromatic residues Y55, F77, W86, and F126 for Mip and Y26, F46, W59, and F99 for FKBP12 (Figure 4). Interestingly, the other parts of the binding domain interacted with different Mip residues during the simulation. A greater number of Mip residues were engaged in interactions with rapamycin, leading to a larger surface area of rapamycin being covered by Mip compared to FKBP12. This confirms the strong immunosuppressant effect of rapamycin, which would be counterproductive for the treatment of Legionaire's disease. More flexible ligands should exhibit better binding ability to Mip than to FKBP12.

4. Conclusion

The combined classical and flooding dynamic simulation approach can reveal the differences between the Mip-rapamycin and the complex FKBP12-rapamycin complexes. This study found that the dynamic features of FKBP12-rapamycin were different from those of Mip-rapamycin. The RMSD analysis showed that the Mip-rapamycin complex was more flexible than the FKBP12-rapamycin complex, and the RMSF studies revealed that the maximum deviations of Mip were seen in the regions 8 and 13 where the binding site residues are located, whereas those of FKBP12 only in the region 13. Furthermore, by applying dPCA to MD trajectories to provide a free energy landscape, six and three conformations were obtained and visualized for the Mip-rapamycin and FKBP12 complexes, respectively. The conformers of Mip showed different interactions within the binding domain of rapamycin, while the three conformers of FKBP12 revealed similar interactions with rapamycin. The lower flexibility of FKBP12 is due to intramolecular hydrogen-bond interactions of the binding site residues Y26, D37, and R42 and one water molecule trapped in the binding pocket. The flooding simulation enhanced the conformational space of Mip-rapamycin and FKBP12-rapamycin complexes. The findings are interesting and confirm many points that our findings may be helpful for the discovery of selective Mip inhibitors. Future work may consider the binding of other ligands to these FKBP proteins.

Acknowledgment

This research has been funded by the German Academic Exchange Service (DAAD) and Widya Mandala Catholic University Surabaya. We also thank Professor Christoph Sotriffer (University of Wuerzburg, Germany) for support in the initial stages of this project.

References

[1] Victor L. Yu, Joseph F. Plouffe, Maddalena Castellani Pastoris, Janet E. Stout, Mona Schousboe, Andreas Widmer, James Summersgill, Thomas File, Christopher M. Heath, David L. Paterson, Annette Chereshsky, Distribution of *Legionella* Species and Serogroups Isolated by Culture in Patients with Sporadic Community-Acquired Legionellosis: An International Collaborative Survey, *The Journal of Infectious Diseases*, 186, 1, (2002), 127-128 https://doi.org/10.1086/341087

[2] Andrea L. Benin, Robert F. Benson, Richard E. Besser, Trends in Legionnaires Disease, 1980–1998: Declining Mortality and New Patterns of Diagnosis, *Clinical Infectious Diseases*, 35, 9, (2002), 1039-1046 https://doi.org/10.1086/342903

[3] Nabi Jomehzadeh, Mojtaba Moosavian, Morteza Saki, Mohammad Rashno, Legionella and legionnaires' disease: An overview, *Journal of Acute Disease*, 8, 6, (2019), 221-232 https://doi.org/10.4103/2221-6189.272853

[4] Thomas J. Marrie, Paul S. Hoffman, Chapter 32 - Legionellosis, in: R.L. Guerrant, D.H. Walker, P.F. Weller (Eds.) *Tropical Infectious Diseases: Principles, Pathogens and Practice (Third Edition)*, W.B. Saunders, Edinburgh, 2011, https://doi.org/10.1016/B978-0-7020-3935-5.00032-X

[5] J. Rasch, C. M. Ünal, A. Klages, Ü. Karsli, N. Heinsohn, R. M. H. J. Brouwer, M. Richter, A. Dellmann, M. Steinert, Peptidyl-Prolyl-*cis/trans*-Isomerases Mip and PpiB of *Legionella pneumophila* Contribute to Surface Translocation, Growth at Suboptimal Temperature, and Infection, *Infection and Immunity*, 87, (2019), e00939-00917 https://doi.org/10.1128/iai.00939-17

[6] Jadwiga Winiecka-Krusnell, Ewert Linder, Free-living Amoebae Protecting Legionella in Water: The Tip of an Iceberg?, *Scandinavian Journal of Infectious Diseases*, 31, 4, (1999), 383-385 https://doi.org/10.1080/00365549950163833

[7] Andreas Ceymann, Martin Horstmann, Philipp Ehses, Kristian Schweimer, Anne-Katrin Paschke, Michael Steinert, Cornelius Faber, Solution structure of the *Legionella pneumophila* Mip-

rapamycin complex, *BMC Structural Biology*, 8, (2008), 17 https://doi.org/10.1186/1472-6807-8-17

[8] Gregory D. Van Duyne, Robert F. Standaert, Stuart L. Schreiber, Jon Clardy, Atomic structure of the rapamycin human immunophilin FKBP-12 complex, *Journal of the American Chemical Society*, 113, 19, (1991), 7433-7434 https://doi.org/10.1021/ja00019a057

[9] Matthew W. Harding, Andrzej Galat, David E. Uehling, Stuart L. Schreiber, A receptor for the immuno-suppressant FK506 is a cis–trans peptidyl-prolyl isomerase, *Nature*, 341, 6244, (1989), 758-760 https://doi.org/10.1038/341758a0

[10] Jürgen M. Kolos, Andreas M. Voll, Michael Bauder, Felix Hausch, FKBP Ligands—Where We Are and Where to Go?, *Frontiers in Pharmacology*, 9, (2018), 1425 https://doi.org/10.3389/fphar.2018.01425

[11] John J. Siekierka, Shirley H. Y. Hung, Martin Poe, C. Shirley Lin, Nolan H. Sigal, A cytosolic binding protein for the immunosuppressant FK506 has peptidyl-prolyl isomerase activity but is distinct from cyclophilin, *Nature*, 341, (1989), 755-757 https://doi.org/10.1038/341755a0

[12] Robert Cafferkey, Peter R. Young, Megan M. McLaughlin, Derk J. Bergsma, Yigal Koltin, Ganesh M. Sathe, Leo Faucette, Wai-Kwong Eng, Randall K. Johnson, George P. Livi, Dominant Missense Mutations in a Novel Yeast Protein related to Mammalian Phosphatidylinositol 3-Kinase and VPS34 Abrogate Rapamycin Cytotoxicity, *Molecular and Cellular Biology*, 13, 10, (1993), 6012-6023 https://doi.org/10.1128/mcb.13.10.6012-6023.1993

[13] Joseph Heitman, N. Rao Movva, Michael N. Hall, Targets for Cell Cycle Arrest by the Immunosuppressant Rapamycin in Yeast, *Science*, 253, 5022, (1991), 905-909 https://doi.org/10.1126/science.1715094

[14] Jeannette Kunz, Ruben Henriquez, Ulrich Schneider, Maja Deuter-Reinhard, N. Rao Movva, Michael N. Hall, Target of rapamycin in yeast, TOR2, is an essential phosphatidylinositol kinase homolog required for G_1 progression, *Cell*, 73, 3, (1993), 585-596 https://doi.org/10.1016/0092-8674(93)90144-F

[15] Mingming Tong, Yu Jiang, FK506-Binding Proteins and Their Diverse Functions, *Current Molecular Pharmacology*, 9, (2016), 48-65 http://dx.doi.org/10.2174/1874467208666150519113541

[16] Janine Rasch, Martin Theuerkorn, Can Ünal, Natascha Heinsohn, Stefan Tran, Gunter Fischer, Matthias Weiwad, Michael Steinert, Novel Cycloheximide Derivatives Targeting the Moonlighting Protein Mip Exhibit Specific Antimicrobial Activity Against *Legionella pneumophila*, *Frontiers in Bioengineering and Biotechnology*, 3, 41, (2015), https://doi.org/10.3389/fbioe.2015.00041

[17] Maral Aminpour, Carlo Montemagno, Jack A. Tuszynski, An Overview of Molecular Modeling for Drug Discovery with Specific Illustrative Examples of Applications, *Molecules*, 24, 9, (2019), 1693 https://doi.org/10.3390/molecules24091693

[18] Emilia P. Barros, Jamie M. Schiffer, Anastassia Vorobieva, Jiayi Dou, David Baker, Rommie E. Amaro, Improving the Efficiency of Ligand-Binding Protein Design with Molecular Dynamics Simulations, *Journal of Chemical Theory and Computation*, 15, 10, (2019), 5703-5715 https://doi.org/10.1021/acs.jctc.9b00483

[19] Hideaki E. Kato, Yoon Seok Kim, Joseph M. Paggi, Kathryn E. Evans, William E. Allen, Claire Richardson, Keiichi Inoue, Shota Ito, Charu Ramakrishnan, Lief E. Fenno, Keitaro Yamashita, Daniel Hilger, Soo Yeun Lee, Andre Berndt, Kang Shen, Hideki Kandori, Ron O. Dror, Brian K. Kobilka, Karl Deisseroth, Structural mechanisms of selectivity and gating in anion channelrhodopsins, *Nature*, 561, 7723, (2018), 349-354 https://doi.org/10.1038/s41586-018-0504-5

[20] Aashish Manglik, Henry Lin, Dipendra K. Aryal, John D. McCorvy, Daniela Dengler, Gregory Corder, Anat Levit, Ralf C. Kling, Viachaslau Bernat, Harald Hübner, Xi-Ping Huang, Maria F. Sassano, Patrick M. Giguère, Stefan Löber, Duan Da, Grégory Scherrer, Brian K. Kobilka, Peter Gmeiner, Bryan L. Roth, Brian K. Shoichet, Structure-based discovery of opioid analgesics with reduced side effects, *Nature*, 537, (2016), 185-190 https://doi.org/10.1038/nature19112

[21] Gleb Solomentsev, Carl Diehl, Mikael Akke, Conformational Entropy of FK506 Binding to FKBP12 Determined by Nuclear Magnetic Resonance Relaxation and Molecular Dynamics Simulations, *Biochemistry*, 57, 9, (2018), 1451-1461 https://doi.org/10.1021/acs.biochem.7b01256

[22] Lilian Olivieri, Fabrice Gardebien, Structure-Affinity Properties of a High-Affinity Ligand of FKBP12 Studied by Molecular Simulations of a Binding Intermediate, *PLoS ONE*, 9, 12, (2014), e114610 https://doi.org/10.1371/journal.pone.0114610

[23] Scott A. Hollingsworth, Ron O. Dror, Molecular Dynamics Simulation for All, *Neuron*, 99, 6, (2018), 1129-1143 https://doi.org/10.1016/j.neuron.2018.08.011

[24] Helmut Grubmüller, Predicting slow structural transitions in macromolecular systems: Conformational flooding, *Physical Review E*, 52, 3, (1995), 2893-2906 https://doi.org/10.1103/PhysRevE.52.2893

[25] Oliver F. Lange, Lars V. Schäfer, Helmut Grubmüller, Flooding in GROMACS: Accelerated barrier crossings in molecular dynamics, *Journal of Computational Chemistry*, 27, 14, (2006), 1693-1702 https://doi.org/10.1002/jcc.20473

[26] Brita G. Schulze, Helmut Grubmüller, Jeffrey D. Evanseck, Functional Significance of Hierarchical Tiers in Carbonmonoxy Myoglobin: Conformational Substates and Transitions Studied by Conformational Flooding Simulations, *Journal of the American Chemical Society*, 122, 36, (2000), 8700-8711 https://doi.org/10.1021/ja993788y

[27] Junmei Wang, Romain M. Wolf, James W. Caldwell, Peter A. Kollman, David A. Case, Development and testing of a general amber force field, *Journal of Computational Chemistry*, 25, 9, (2004), 1157-1174 https://doi.org/10.1002/jcc.20035

[28] D Case, I Ben-Shalom, S Brozell, D Cerutti, T III Cheatham, V Cruzeiro, T Darden, R Duke, D Ghoreishi, M.K. Gilson, H. Gohlke, A.W. Goetz, D.

Greene, R Harris, N. Homeyer, Y. Huang, S. Izadi, A. Kovalenko, T. Kurtzman, T.S. Lee, S. LeGrand, P. Li, C. Lin, J. Liu, T. Luchko, R. Luo, D.J. Mermelstein, K.M. Merz, Y. Miao, G. Monard, C. Nguyen, H. Nguyen, I. Omelyan, A. Onufriev, F. Pan, R. Qi, D.R. Roe, A. Roitberg, C. Sagui, S. Schott-Verdugo, J. Shen, C.L. Simmerling, J. Smith, R. Salomon-Ferrer, J. Swails, R.C. Walker, J. Wang, H. Wei, R.M. Wolf, X. Wu, L. Xiao, D.M. York, P.A. Kollman, *Amber 2018*, University of California, San Francisco, 2018,

[29] Alan W. Sousa da Silva, Wim F. Vranken, ACPYPE - AnteChamber PYthon Parser interfacE, *BMC Research Notes*, 5, (2012), 367 https://doi.org/10.1186/1756-0500-5-367

[30] Junmei Wang, Wei Wang, Peter A. Kollman, David A. Case, Automatic atom type and bond type perception in molecular mechanical calculations, *Journal of Molecular Graphics and Modelling*, 25, 2, (2006), 247-260 https://doi.org/10.1016/j.jmgm.2005.12.005

[31] M. J. Abraham, D. Van Der Spoel, E. Lindahl, B. Hess, in, 2018,

[32] Henk Bekker, H. J. C. Berendsen, E. J. Dijkstra, S. Achterop, R. Vondrumen, David Vanderspoel, A. Sijbers, H. Keegstra, M. K. R. Renardus, Gromacs: A parallel computer for molecular-dynamics simulations, *4th International Conference on Computational Physics (PC 92)*, 1993

[33] H. J. C. Berendsen, D. van der Spoel, R. van Drunen, GROMACS: A message-passing parallel molecular dynamics implementation, *Computer Physics Communications*, 91, 1, (1995), 43-56 https://doi.org/10.1016/0010-4655(95)00042-E

[34] Berk Hess, Carsten Kutzner, David van der Spoel, Erik Lindahl, GROMACS 4: Algorithms for Highly Efficient, Load-Balanced, and Scalable Molecular Simulation, *Journal of Chemical Theory and Computation*, 4, 3, (2008), 435-447 https://doi.org/10.1021/ct700301q

[35] Erik Lindahl, Berk Hess, David van der Spoel, GROMACS 3.0: a package for molecular simulation and trajectory analysis, *Molecular modeling annual*, 7, (2001), 306-317 https://doi.org/10.1007/s008940100045

[36] Szilárd Páll, Mark James Abraham, Carsten Kutzner, Berk Hess, Erik Lindahl, Tackling Exascale Software Challenges in Molecular Dynamics Simulations with GROMACS, *Solving Software Challenges for Exascale*, Cham, 2015 https://doi.org/10.1007/978-3-319-15976-8_1

[37] Sander Pronk, Szilárd Páll, Roland Schulz, Per Larsson, Pär Bjelkmar, Rossen Apostolov, Michael R. Shirts, Jeremy C. Smith, Peter M. Kasson, David van der Spoel, Berk Hess, Erik Lindahl, GROMACS 4.5: a high-throughput and highly parallel open source molecular simulation toolkit, *Bioinformatics*, 29, 7, (2013), 845-854 https://doi.org/10.1093/bioinformatics/btt055

[38] David Van Der Spoel, Erik Lindahl, Berk Hess, Gerrit Groenhof, Alan E. Mark, Herman J. C. Berendsen, GROMACS: Fast, flexible, and free, *Journal of Computational Chemistry*, 26, 16, (2005), 1701-1718 https://doi.org/10.1002/jcc.20291

[39] Kresten Lindorff-Larsen, Stefano Piana, Kim Palmo, Paul Maragakis, John L. Klepeis, Ron O. Dror, David E. Shaw, Improved side-chain torsion potentials for the Amber ff99SB protein force field, *Proteins: Structure, Function, and Bioinformatics*, 78, 8, (2010), 1950-1958 https://doi.org/10.1002/prot.22711

[40] William L. Jorgensen, Jayaraman Chandrasekhar, Jeffry D. Madura, Roger W. Impey, Michael L. Klein, Comparison of simple potential functions for simulating liquid water, *The Journal of Chemical Physics*, 79, (1983), 926-935 https://doi.org/10.1063/1.445869

[41] Tom Darden, Darrin York, Lee Pedersen, Particle mesh Ewald: An *N*·log(*N*) method for Ewald sums in large systems, *The Journal of Chemical Physics*, 98, (1993), 10089-10092 https://doi.org/10.1063/1.464397

[42] Giovanni Bussi, Davide Donadio, Michele Parrinello, Canonical sampling through velocity rescaling, *The Journal of Chemical Physics*, 126, (2007), 014101 https://doi.org/10.1063/1.2408420

[43] M. Parrinello, A. Rahman, Polymorphic transitions in single crystals: A new molecular dynamics method, *Journal of Applied Physics*, 52, (1981), 7182-7190 https://doi.org/10.1063/1.328693

[44] Shuichi Miyamoto, Peter A. Kollman, Settle: An analytical version of the SHAKE and RATTLE algorithm for rigid water models, *Journal of Computational Chemistry*, 13, 8, (1992), 952-962 https://doi.org/10.1002/jcc.540130805

[45] Jean-Paul Ryckaert, Giovanni Ciccotti, Herman J. C. Berendsen, Numerical integration of the cartesian equations of motion of a system with constraints: molecular dynamics of n-alkanes, *Journal of Computational Physics*, 23, 3, (1977), 327-341 https://doi.org/10.1016/0021-9991(77)90098-5

[46] Justin A. Lemkul, From Proteins to Perturbed Hamiltonians: A Suite of Tutorials for the GROMACS-2018 Molecular Simulation Package [Article v1.0], *Living Journal of Computational Molecular Science*, 1, 1, (2019), 5068 https://doi.org/10.33011/livecoms.1.1.5068

[47] Benjamin Bouvier, Helmut Grubmüller, A Molecular Dynamics Study of Slow Base Flipping in DNA using Conformational Flooding, *Biophysical Journal*, 93, 3, (2007), 770-786 https://doi.org/10.1529/biophysj.106.091751

[48] Gareth A. Tribello, Michele Ceriotti, Michele Parrinello, A self-learning algorithm for biased molecular dynamics, *Proceedings of the National Academy of Sciences*, 107, 41, (2010), 17509-17514 https://doi.org/10.1073/pnas.1011511107

[49] Alexandros Altis, Phuong H. Nguyen, Rainer Hegger, Gerhard Stock, Dihedral angle principal component analysis of molecular dynamics simulations, *The Journal of Chemical Physics*, 126, 24, (2007), 244111 https://doi.org/10.1063/1.2746330

[50] Alexandros Altis, Moritz Otten, Phuong H. Nguyen, Rainer Hegger, Gerhard Stock, Construction of the free energy landscape of biomolecules via dihedral angle principal component analysis, *The Journal of Chemical Physics*, 128, (2008), 245102 https://doi.org/10.1063/1.2945165

[51] Jun Liang, Jungwon Choi, Jon Clardy, Refined structure of the FKBP12–rapamycin–FRB ternary complex at 2.2 Å resolution, *Acta Crystallographica Section D: Biological Crystallography*, 55, 4, (1999),

736-744
https://doi.org/10.1107/S0907444998014747

[52] Harvey Lodish, Arnold Berk, S. Lawrence Zipursky, Paul Matsudaira, David Baltimore, James Darnell, Noncovalent bonds, in: *Molecular Cell Biology*, W. H. Freeman, 2000,

[53] S. Gaali, R. Gopalakrishnan, Y. Wang, C. Kozany, F. Hausch, The Chemical Biology of Immunophilin Ligands, *Current Medicinal Chemistry*, 18, 35, (2011), 5355-5379
http://dx.doi.org/10.2174/092986711798194342

[54] BIOVIA, Discovery Studio Visualizer, Dassault Systèmes, (2020), https://3ds.com/products-services/biovia/products

[55] William Humphrey, Andrew Dalke, Klaus Schulten, VMD: Visual molecular dynamics, *Journal of Molecular Graphics*, 14, 1, (1996), 33-38
https://doi.org/10.1016/0263-7855(96)00018-5